

*Accepted November 19<sup>th</sup> 2022*

**PASSIVE TRACER TRANSPORT IN PERISTALTIC PUMPING OF  
NON-NEWTONIAN BLOOD FLOW: A MATHEMATICAL MODEL**

O. Anwar Béq CMath FIMA<sup>1\*</sup> and Ashis Kumar Roy<sup>2</sup>

<sup>1</sup>Professor, Multi-Physical Engineering Sciences Group, Mechanical Engineering Department, Corrosion Lab, 3-08, SEE Building, University of Salford, Manchester, M5 4WT, UK. [O.A.Beg@salford.ac.uk](mailto:O.A.Beg@salford.ac.uk)

<sup>2</sup>Department of Science and Humanities, Tripura Institute of Technology, Narsingarh, Tripura -799009, India.

**Abstract:** The large time behaviour of passive contaminant in non-Newtonian peristaltic blood flow in a two-dimensional channel (capillary) has been examined in the present article. The power-law model is employed in order to highlight the non-Newtonian blood characteristic. The study was conducted using the Reynolds decomposition technique, which converts a two-dimensional transport problem into a one-dimensional transport model in which species concentration can be decomposed into sectional average concentration and variation from its mean value. For flow velocity, the same decomposition method is used. This allows the derivation of the dispersion coefficient and convection coefficient. Using Fick's law, the advection-diffusion equation is modified by replacing these coefficients by their corresponding average values and analytical solutions for the mean concentration are derived. In the absence of peristalsis effects ( $\gamma = 0$ ) i.e., for the straight rigid channel, the dispersion coefficient is invariant along the channel length. With increasing modulation (peristaltic wave) parameter,  $\gamma$ , there is a strong elevation in advection coefficient in the initial half of the channel with a subsequent suppression in the second half of the channel, indicating that the location in the channel strongly influences advection characteristics. Advection coefficient is significantly elevated with increment in power-law rheological index (for shear-thinning fluids,  $n < 1$ ) across the channel length and exhibits an oscillatory nature due to the peristaltic waves. In the shear-thickening range ( $n > 1$ ), with progressive increase in  $n$ , an increment in peristaltic modulation parameter,  $\gamma$ , induces a marked reduction in the axially average relative advection coefficient. Dispersion coefficient is initially boosted along the early section of the channel with increment in modulation parameter whereas further long the channel this trend is reversed. Increasing aspect ratio and Péclet number consistently boost dispersion coefficient along the entire channel length. The study provides a solid benchmark for further generalized simulations with computational fluid dynamics.

**Keywords:** *Peristaltic pumping; blood flow; power-law model; mean concentration; advection coefficient; dispersion coefficient*

## Nomenclature

$C(x, y, t)$	solute concentration
$d$	semi – width of channel
$D$	molecular diffusion coefficient
$D(x)$	dispersion coefficient
$h$	half of separation width between the two walls
$K$	flow consistency
$K_1$	advection coefficient
$n$	flow behavior index
$p$	pressure
$Pe$	Péclet number
$t$	time
$u(x, y)$	flow velocity
$\langle u \rangle$	transversely average velocity
$v_{\text{wave}}$	speed of peristaltic wave
$x$	axial coordinate
$y$	transverse coordinate

### *Greek symbols*

$\epsilon$	aspect ratio
$\gamma$	modulation parameter
$\lambda$	wavelength of peristaltic wave
$\mu_{\text{eff}}$	apparent viscosity
$\tau$	stress

### *Superscripts*

'	dimensionless
~	deviation from average

### *Subscript*

$N$	Newtonian case
-----	----------------

## 1.Introduction

Peristalsis is a fundamental mechanism utilized in biological transport. It arises in many internal flow applications including blood flow in capillaries [1], gastric pumping etc. In peristaltic flows in biological conduits e. g. blood vessels, longitudinally oriented muscle in the segment ahead of the advancing intraluminal contents contracts while the circumferentially oriented muscle layer relaxes in the same segment. Simultaneous shortening of the longitudinal axis and relaxation of the circular muscle result in expansion of the lumen and peristaltic waves are

generated along the vessel walls producing a very efficient propulsion mechanism. Peristalsis also arises in airway transport [2] and swallowing dynamics (esophageal flows) [3]. It has also been explored as a very efficient mechanism in biomimetic pumps for pharmacology [4] and also cardiopulmonary bypass blood supply [5]. Fundamental studies of Newtonian peristaltic flow were conducted by Jaffrin and Shapiro [6] who introduced lubrication approximations i.e., long wavelength and low Reynolds numbers to develop simplified solutions for peristaltic pumping dynamics. However, they did not consider non-Newtonian effects which have been shown to be important in smaller blood vessels where the rheological characteristics of blood cannot be neglected [7]. In recent years many excellent studies [] have therefore been communicated which examine peristaltic transport in non-Newtonian fluids and utilize many different rheological models. Raju and Devanathan [8] generalized the Jaffrin-Shapiro model [6] to consider the peristaltic motion of a power law fluid in a tube, with a sinusoidal wave of small amplitude. They derived solutions for the stream function is obtained as a power series in terms of the amplitude of the wave and investigated the effects of the applied pressure gradient along with non-Newtonian parameters on the streamlines and velocity profiles. Tripathi *et al.* [9] studied viscoelastic slip flow in peristaltic propulsion with the Oldroyd-B model and a homotopy method. Another method, namely, the Direct-forcing immersed boundary–non-Newtonian lattice Boltzmann method (IB–NLBM) has also been used by several authors [10,11,12] to investigate the sedimentation and interaction of particles in different fluid models. Suresh and Hemadri [13] reviewed the accuracy of a variety of non-Newtonian models including viscoplastic Casson and power-law models for pharmacological peristaltic transport. Maiti and Misra [14] studied theoretically the Herschel–Bulkley rheological peristaltic flow of blood through a micro-vessel (arteriole) of variable cross-section. They noted that flow velocity and wall shear stress are strongly modified by non-uniformity of the cross-sectional radius of the blood vessel of the micro-circulatory system and that the peristaltic transport is significantly influenced by wave amplitude ratio and non-Newtonian power-law index. They also observed that backward flow is produced by contraction of vessels and a higher possibility of trapping is associated with higher power-law index. Furthermore, they identified that retrograde flow region is sustained for negative or zero pressure difference for Herschel–Bulkley fluids, and that shear stress difference between outlet and inlet in converging vessels is greater for the shear-thickening case. Tripathi and Bég [15] used a homotopy perturbation method (HPM) to investigate the peristaltic transport of generalized Maxwell viscoelastic fluids through a Darcy-Brinkman porous medium in a diseased blood vessel. They noted that in the entire pumping region and the free pumping region, both volumetric flow rate and pressure are suppressed with increasing viscoelastic relaxation time, whereas in the co-pumping region, the volumetric flow rate is enhanced strongly with

increment in relaxation time. They also observed that the trapped bolus is expanded by with greater permeability of the porous medium but reduced with higher peristaltic wave amplitude ratio. Usha and Ramachandra [16] studied theoretically the peristaltic pumping of two-layered power-law fluids in axisymmetric tubes. They showed that a negative time-mean flow is produced in free pumping (zero pressure difference case) when one of peripheral layer and core fluids is non-Newtonian. They also noted that noticed that a sinusoidal wave generally produces a positive mean flow for power-law fluids and that the size of the trapped bolus volume is smaller for shear thinning cases in the core and the peripheral layer fluids. Further studies have examined peristaltic propulsion of Herschel Bulkley fluid in an inclined tube [17], Carreau shear-dependent viscosity peristaltic flows in a curved channel [18], peristalsis in Casson biofluids [19, 20] and Vocadlo viscoplastic peristaltic dynamics [21]. All these investigations have confirmed the significant influence of non-Newtonian blood characteristics on wall shear stress, pressure distribution and hydromechanical efficiency in peristaltic wave propagation vessels.

Blood is a complex fluid which in addition to featuring rheological behaviour in micro-vessels also contains many suspensions. These include ions, proteins, oxygen, nutrients etc. Solute transport is an essential function of blood and involves mass transfer i.e., *species diffusion and convection*. It is also relevant to transport of drugs or toxins in physiological systems and bio-, chromatographic separations in medical engineering processing devices. When a solute is present in blood, it is convected and dispersed within the blood stream. Mathematical models of dispersion in blood flow are critical to understanding the fate of solutes. For example, in pharmacodynamics, these models can improve our understanding of the fate of drugs and their efficacy. The solute dispersion process in a Newtonian fluid in a rigid cylindrical vessel was first addressed by Taylor [22] who identified that the solute is dispersed owing to molecular diffusion and computed the variation in the velocity over the cross section. This constitutes the classical Taylor hydrodynamic dispersion theory. Later, Aris [23] generalized the Taylor dispersion model for both steady and pulsatile flows using the method of moments. Gill & Sankarasubramanian [24] further improved the Aris-Taylor model to consider solute dispersion at small and large times, in which an improved solution for the time-dependent dispersion coefficient, which tends to Taylor-Aris's diffusion coefficient at large time, was derived using the series expansion technique. They also showed that following the injection of solute at small time, the axial dispersion process is principally dictated by the axial convection of solute rather than the transverse diffusion. However at large times, the solute transport is more dominated by molecular diffusion. A number of clinical and analytical studies of dispersion in blood have also been communicated. Lane and Sirs [25] investigated the dispersion of solutes in plasma and blood has been studied by observing the clearance at a point down-stream of a bolus of labelled

solution by the steady flow of unlabelled solution. They showed that dispersion of solutes during blood flow through a straight tube is controlled by the combined effects of solute diffusion and laminar convection, and motion of the erythrocytes may contribute to mixing, in the bulk of the flow. Caro [26] examined the dispersion of indicator flowing through blood vessels with a focus on velocity modification. Roy *et al.* [27] studied the hydrodynamic dispersion in reactive drug transport in a blood vessel containing a non-Darcy porous medium. They showed that higher values of reaction parameter and Forchheimer (non-Darcy) number suppress the dispersion coefficient and that maximum mean concentration is enhanced with greater Forchheimer numbers, although the centre of the solute cloud is displaced in the backward direction. They further observed that peak mean concentration is decreased over time since the dispersion process is largely dominated by diffusion at the large time. These studies however were confined to Newtonian flows. Non-Newtonian hydrodynamic dispersion however is more representative of actual micro-vessel blood flows. Early work in non-Newtonian dispersion was motivated by chemical engineering developments and interesting studies were presented by Fan and Wang [28] and later by Dejam [29] for power-law fluids, Shah and Cox [30] for Casson fluids and later Sharp [31] for additionally Bingham viscoplastic (yield stress) fluids. More recently Roy and Bég [32] considered transient Taylor reactive dispersion in two-fluid (micropolar and Newtonian) blood flow. They used the Gill decomposition method for the concentration field. They observed that transverse concentration is boosted with increasing micropolar coupling number and reaction rate. They also noted that transverse concentration is boosted with increasing micropolar coupling number and reaction rate; however, whereas it is suppressed with greater micropolar material parameter and viscosity ratio. Additionally, axial mean concentration peaks are reduced in magnitude and pushed further along the vessel length and also dispersion coefficient is reduced with increasing micropolar material parameter whereas it is boosted with a greater viscosity ratio. Bég and Roy [33] further investigated dual *component species convective-diffusion transport in non-Newtonian blood flow with bulk chemical reaction through a two-dimensional rigid vessel* is with the yield stress Casson fluid model. Two different bulk degradation reaction rates are included for the dual species (pharmacological agents, *A*, *B*). Further studies have been reported by Saadun *et al.* [34] who deployed the Bingham model and considered body acceleration effects in hydrodynamic dispersion in rheological blood flow. Rana and Murthy [35] deployed a two-phase Casson viscoplastic model to compute the dispersion of solute in an unsteady blood flow in small arteries with and without absorption at the wall. They showed that mean concentration of solute is decreased with increasing radius of the vessels and with decreasing values of *Schmidt number*, the molecular diffusion becomes more effective in the solute dispersion process, and this leads to an increase in axial

dispersion. Ponalagusamy and Murugan [36] analyzed the Taylor dispersion of a solute in blood flow in a tube using a thixotropic non-Newtonian model and including homogeneous chemical reaction. They showed that the dispersion coefficient is reduced with greater reaction rate constant whereas with increment in thixotropic parameter reduces the equivalent dispersion coefficient.

The above studies did not simultaneously consider *peristaltic non-Newtonian blood flow* with *hydrodynamic dispersion*. This is the focus of the present study. The Ostwald-DeWaele power-law model is deployed. This model can accommodate both shear thinning in blood and also shear thickening. The latter *may arise for example when there is* an imbalance in the proteins and cells responsible for blood and blood clotting develops, the blood can become too thick. This is known as *hypercoagulability* and is characterized by shear-thickening. Therefore, the power-law model is also appropriate for simulating such blood flows. In previous studies alternate non-Newtonian models have been considered for dispersion in peristaltic blood flows including the Stokes couple stress model [37] and the Eringen micropolar model [38]. In the present work, a novel investigation is conducted for hydrodynamic dispersion in non-Newtonian peristaltic blood flow in a two-dimensional channel with boundary chemical reaction, as a simulation of solute transport in capillaries. A velocity solution is derived for generalized power-law index. The unsteady convective diffusive equation for concentration of solute is then formulated with appropriate boundary conditions. Appropriate transformations are deployed to render the model non-dimensional. Convection is assumed to be dominant compared to the axial diffusion. Reynolds' decomposition technique is applied in order to convert reduce the two-dimensional solute transport model into an equivalent one-dimensional model, in which the chemical species concentration and velocity in the channel can be considered as the sum of the cross-sectional average values and their deviations from the averages. This allows the derivation of the *dispersion coefficient and convection coefficient*. Using Fick's law, the advection-diffusion equation is modified by replacing these coefficients by their corresponding average values and analytical solutions for the mean concentration are derived. The effects of peristaltic modulation parameter ( $\gamma$ ) and power-law index ( $n$ ) on both advection and dispersion coefficients is computed along the channel length. Both shear thinning blood ( $n < 1$ ) and shear-thickening blood ( $n > 1$ ) are investigated. The analysis presented is relevant to broadening the clinical understanding of the influence of rheology in peristaltic blood flows [39, 40].

## 2. Mathematical Model

In the present model we consider solute dispersion process in peristaltic propulsion of non-Newtonian power-law fluid through a uniform 2-D channel (micro-blood vessel) having width  $2d$  and oscillating walls. The channel oscillations are imposed by traveling sinusoidal waves of long wavelength  $\lambda$  which propagate along the distensible channel walls, and obey the following relation [38]:

$$y = \pm h = \pm \left[ d + a \sin \frac{2\pi}{\lambda} (x - v_{\text{wave}} t) \right] \quad (1)$$

Here  $a$  is the amplitude, and  $v_{\text{wave}}$  is the speed of the peristaltic wave. The geometrical configuration is displayed in **Fig. 1**.

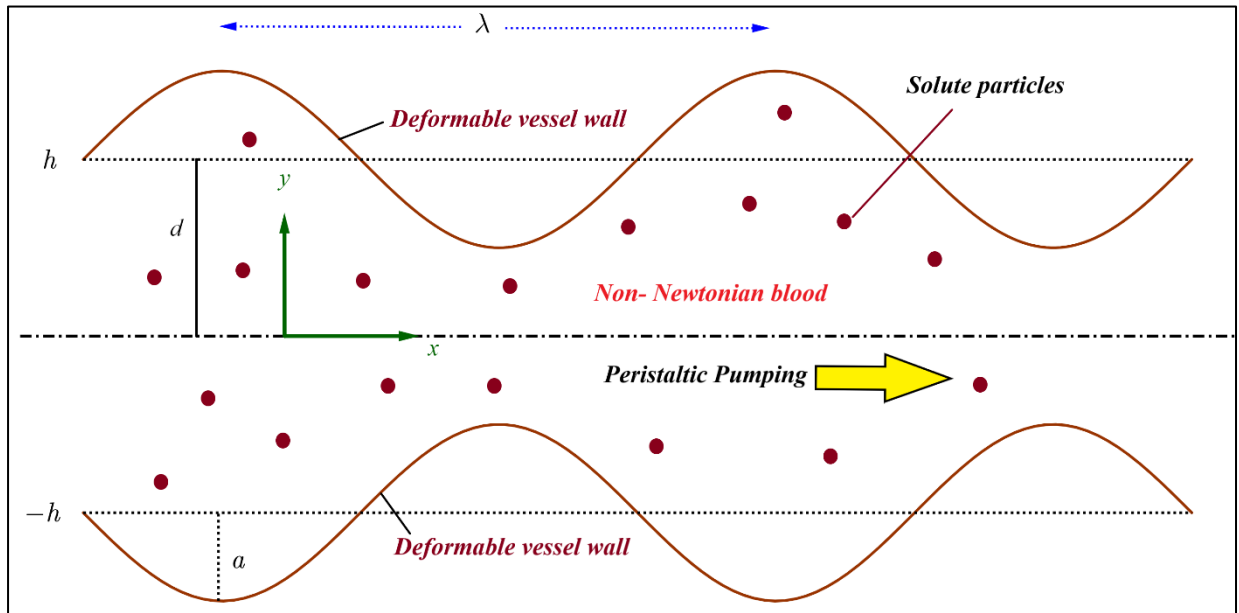


Figure 1: Schematic diagram of the model geometry.

By virtue of these assumptions, the governing equation of motion for steady blood flow is:

$$\frac{\partial \tau}{\partial y} = \frac{\partial p}{\partial x} \quad (2)$$

The symbol  $p, \tau, u$  symbolize the pressure, stress and axial velocity respectively.

The constitutive equation for power-law non-Newtonian fluids, in one dimensional shear flow may be written as:

$$\tau = K \left( \frac{\partial u}{\partial y} \right)^n \quad (3)$$

Here  $K$  is the flow consistency index and  $n$  is the flow behavior index (dimensionless). Combination of Eqn. (1) and  $\tau = \mu_{\text{eff}} \partial u / \partial y$  results in the apparent viscosity,  $\mu_{\text{eff}}$ , for the so-called power law fluid as follows

$$\mu_{\text{eff}} = K \left( \frac{\partial u}{\partial y} \right)^{n-1} \quad (1)$$

It should be noted that the flow behavior index can vary from zero to infinity ( $0 < n < \infty$ ) in theory. For  $0 < n < 1$ , the fluid exhibits *shear-thinning* (or pseudo plastic) behavior where the apparent viscosity decreases with increasing shear rate. Solving (2) using (3) and no slip boundary condition i.e.,  $u = v_{\text{wave}}$  at  $y = \pm h$  we obtain:

$$u(x, y) = v_{\text{wave}} + \frac{nh}{n+1} \left( \frac{h}{K} \frac{dp}{dx} \right)^{\frac{1}{n}} \left[ 1 - \left| \frac{y}{h} \right|^{\frac{n+1}{n}} \right] \quad (2)$$

where  $\langle u \rangle$  is the average velocity.

Associated with above flow scenario, the problem of solute transport (e. g., oxygen) is governed by the unsteady convective diffusive equation [37, 38]:

$$\frac{\partial C}{\partial t} + u \frac{\partial C}{\partial x} = D \left( \frac{\partial^2 C}{\partial x^2} + \frac{\partial^2 C}{\partial y^2} \right), \quad -h < y < h \quad (6)$$

Here  $D$ , the molecular diffusivity of the solute (oxygen) in the fluid, is assumed to be constant.

The initial and boundary conditions are, respectively, given as

$$C(x, y, t) = C_0(x, y) \quad \text{at} \quad t = 0 \quad (7a)$$

$$\frac{\partial C}{\partial y} = 0, \quad \text{at} \quad y = \pm h \quad (7b)$$

$$C(x, y, t) = 0, \quad \text{at} \quad x \rightarrow \pm\infty \quad (7c)$$

Here  $C_0$  is the initial solute concentration.

Introducing the following dimensionless parameters:

$$\begin{aligned}
u' &= \frac{u}{v_{\text{wave}}}, \quad x' = \frac{x}{\lambda} - t', \quad t' = \frac{v_{\text{wave}} t}{\lambda}, \quad y' = \frac{y}{d}, \quad h' = \frac{h}{d}, \quad \gamma = \frac{d}{a}, \\
p' &= p / \frac{K \lambda v_{\text{wave}}^2}{d^{n+1}}, \quad \text{Pe} = \frac{v_{\text{wave}} \lambda}{D}, \quad C' = \frac{C}{C_0},
\end{aligned} \tag{8}$$

In Eqn. (8)  $t'$  denotes the dimensionless variable and Pe is Péclet number. Using the above scaling from Eqn. (8) in Eqns. (3) and (4) we have:

$$\partial_t^2 \frac{\partial C'}{\partial t'} + \partial_x^2 u^* \frac{\partial C'}{\partial x'} = \frac{1}{\text{Pe}} \left( \partial_x^2 \frac{\partial^2 C'}{\partial x'^2} + \frac{\partial^2 C'}{\partial y'^2} \right), \tag{9}$$

$$C'(x', y', t') = 1 \quad \text{at} \quad t = 0 \tag{10a}$$

$$\frac{\partial C'}{\partial y'} = 0, \quad \text{at} \quad y = \pm h' \tag{10b}$$

$$C'(x', y', t') = 0, \quad \text{at} \quad x' \rightarrow \pm\infty \tag{10c}$$

Here  $\epsilon$  is aspect ratio of the channel (blood vessel) i.e., length relative to depth. Furthermore, where  $u^* = u' - 1$  and  $h' = 1 + \gamma \sin(2\pi x')$ . For simplicity we have dropped primes hereafter. The appropriate expression for  $u^*$  is:

$$u^* = \frac{nh}{n+1} \left( h \frac{dp}{dx} \right)^{\frac{1}{n}} \left[ 1 - \left( \frac{y}{h} \right)^{\frac{n+1}{n}} \right] \tag{11}$$

## 2.1 Reduced transport model

In the subsequent analysis *Reynolds decomposition technique* is applied in order to reduce the two-dimensional solute transport model into an equivalent one-dimensional model, in which the chemical species concentration and velocity in the channel can be considered as the sum of the cross-sectional average values and their deviations from the averages as given by [29, 41]:

$$C(x, y, t) = \langle C \rangle + \tilde{C}(x, y, t) \tag{12a}$$

$$u(x, y) = \langle u \rangle + \tilde{u}(x, y) \tag{12b}$$

Here the parentheses  $\langle \rangle$  represents the cross-sectional averages of the chemical species concentration and velocity inside the channel, defined as  $\int_0^1 C dy$  and  $\int_0^1 u dy$ , and  $\tilde{C}$  and  $\tilde{u}$  are the corresponding deviations from the averages. Therefore, it follows that:

$$\int_0^h \tilde{C}(x, y, t) dy = 0 \tag{13a}$$

$$\int_0^h \tilde{u}(x, y) dy = 0 \quad (13b)$$

By substitution of Eqn. (12a) into Eqn. (9), the following equation is obtained:

$$\delta^2 \frac{\partial \langle C \rangle}{\partial t} + \delta^2 \frac{\partial \tilde{C}}{\partial t} + \delta^2 u^* \frac{\partial \langle C \rangle}{\partial x} + \delta^2 u^* \frac{\partial \tilde{C}}{\partial x} = \frac{1}{\text{Pe}} \left( \delta^2 \frac{\partial^2 \langle C \rangle}{\partial x^2} + \delta^2 \frac{\partial^2 \tilde{C}}{\partial x^2} + \frac{\partial^2 \tilde{C}}{\partial y^2} \right), \quad (14)$$

The associated initial and boundary conditions emerge as:

$$\langle C \rangle + \tilde{C} = 1 \quad \text{at} \quad t = 0 \quad (15a)$$

$$\frac{\partial \tilde{C}}{\partial y} = 0, \quad \text{at} \quad y = h. \quad (15b)$$

$$\frac{\partial \tilde{C}}{\partial y} = 0, \quad \text{at} \quad y = 0 \quad (15c)$$

$$\langle C \rangle + \tilde{C} = 0, \quad \text{at} \quad x \rightarrow \pm\infty \quad (15d)$$

Taking the cross-sectional average of Eqn. (6) and using the boundary condition at the center of the channel and Eqn. (5) leads to:

$$\frac{\partial \langle C \rangle}{\partial t} + \langle u^* \rangle \frac{\partial \langle C \rangle}{\partial x} + \left\langle u^* \frac{\partial \tilde{C}}{\partial x} \right\rangle = \frac{1}{\text{Pe}} \frac{\partial^2 \langle C \rangle}{\partial x^2}, \quad (16)$$

By virtue of Eqns. (15)-(13) one arrives at the following form of the advection dispersion equation:

$$\frac{\partial \tilde{C}}{\partial t} + [u - \langle u \rangle] \frac{\partial \langle C \rangle}{\partial x} + u^* \frac{\partial \tilde{C}}{\partial x} - \left\langle u^* \frac{\partial \tilde{C}}{\partial x} \right\rangle = \frac{1}{\text{Pe}} \left( \frac{\partial^2 \tilde{C}}{\partial x^2} + \frac{1}{\delta^2} \frac{\partial^2 \tilde{C}}{\partial y^2} \right), \quad (17)$$

In the ensuing analysis, the following three assumptions adopted

- (i) When a sufficient amount of time has passed after the injection of the solute at the channel's inlet i.e.,  $\partial \tilde{C} / \partial t \approx 0$ . This assumption is based on the fact that transverse diffusion smooths out the concentration fluctuations in the vertical direction and this assumption is valid at a time scale  $O(h^2 / D)$
- (ii) The fluctuating component of concentration  $\tilde{C}$ , varies slowly which turns out  $u^* \partial \tilde{C} / \partial x \approx \langle u^* \partial \tilde{C} / \partial x \rangle$ .
- (iii) The convection is dominant compared to the axial diffusion i.e.,  $\tilde{C}_{xx} \ll \text{Pe} u^* \langle C \rangle_x$ .

Incorporating these assumptions leads to:

$$\frac{\partial^2 \tilde{C}}{\partial y^2} = \delta^2 \text{Pe} \frac{nh}{n+1} \left( h \frac{\partial p}{\partial x} \right)^{\frac{1}{n}} \left\{ \frac{n}{2n+1} - \left( \frac{y}{h} \right)^{\frac{n+1}{n}} \right\} \frac{\partial \langle C \rangle}{\partial x} \quad (18)$$

Solving Eqn. (18) using Eqns. (13a) and (15b, c) we obtain:

$$\tilde{C} = \delta^2 \text{Pe} h^2 \langle u^* \rangle \left[ \frac{n}{2(n+1)} \left( \frac{y}{h} \right)^2 - \frac{n^2}{(n+1)(3n+1)} \left( \frac{y}{h} \right)^{\frac{3n+1}{n}} - \frac{n(6n+1)}{6(3n+1)(4n+1)} \right] \frac{\partial \langle C \rangle}{\partial x} \quad (19)$$

Here:

$$\langle u^* \rangle = \frac{nh}{2n+1} \left( h \frac{\partial p}{\partial x} \right)^{\frac{1}{n}} \quad (20)$$

$$\frac{\partial \langle C \rangle}{\partial t} + K_1(x) \frac{\partial C_0 \langle C \rangle}{\partial x} = \frac{1}{\text{Pe}} D(x) \frac{\partial^2 \langle C \rangle}{\partial x^2} \quad (21)$$

Where:

$$D(x) = 1 + \frac{2\delta^2 \text{Pe}^2 n^4 h^4}{3(2n+1)^2 (4n+1)(5n+2)} \left( h \frac{\partial p}{\partial x} \right)^{\frac{2}{n}} \quad (22a)$$

$$K_1(x) = \frac{nh}{2n+1} \left( h \frac{\partial p}{\partial x} \right)^{\frac{1}{n}} \quad (22b)$$

The two coefficients in Eqns. (22a) and (22b) are termed respectively, *dispersion coefficient* and *advection coefficient*. It is important to mention here that these three coefficients are functions of axial co-ordinate. Now when when  $n \rightarrow \infty$  (Newtonian fluid case) these coefficients become:

$$\lim_{n \rightarrow \infty} D(x) = 1 + \frac{\delta^2 \text{Pe}^2 h^4}{120} \quad (23a)$$

$$\lim_{n \rightarrow \infty} K_1(x) = \frac{h}{2} \quad (23b)$$

and well with existing work [42] for straight channel (i.e.,  $h = 1$ ). To analyses the integrated impact of these transport coefficient we take an average *over one wavelength*, i.e.,

$$D^* = \int_0^1 D(x) dx \quad (24a)$$

$$K_1^* = \int_0^1 K_1(x) dx \quad (24b)$$

## 2.2 Mean Concentration

Based on Fick's law, the advection-diffusion equation (Eqn. (22)) can be approximated by replacing the  $K_1(x)$  and  $D(x)$  by their corresponding average values  $K_1^*$  and  $D^*$ . Then the corresponding analytical solution for the advection dispersion blood flow model is given by

$$\langle C \rangle(x,t) = \frac{1}{2} \left[ \operatorname{erfc} \left( \frac{x - K_1^* t}{2\sqrt{D^* t / \text{Pe}}} \right) + \exp \left( \frac{\text{Pe} K_1^* x}{D^*} \right) \operatorname{erfc} \left( \frac{x + K_1^* t}{2\sqrt{D^* t / \text{Pe}}} \right) \right] \quad (25)$$

Numerical evaluation of the dispersion characteristics has been conducted in symbolic software, MATLAB. The computations are presented in the next section for the influence of key parameters on these characteristics in the channel (blood vessel). **Fig. 2** summarizes all key stages of the analysis conducted.

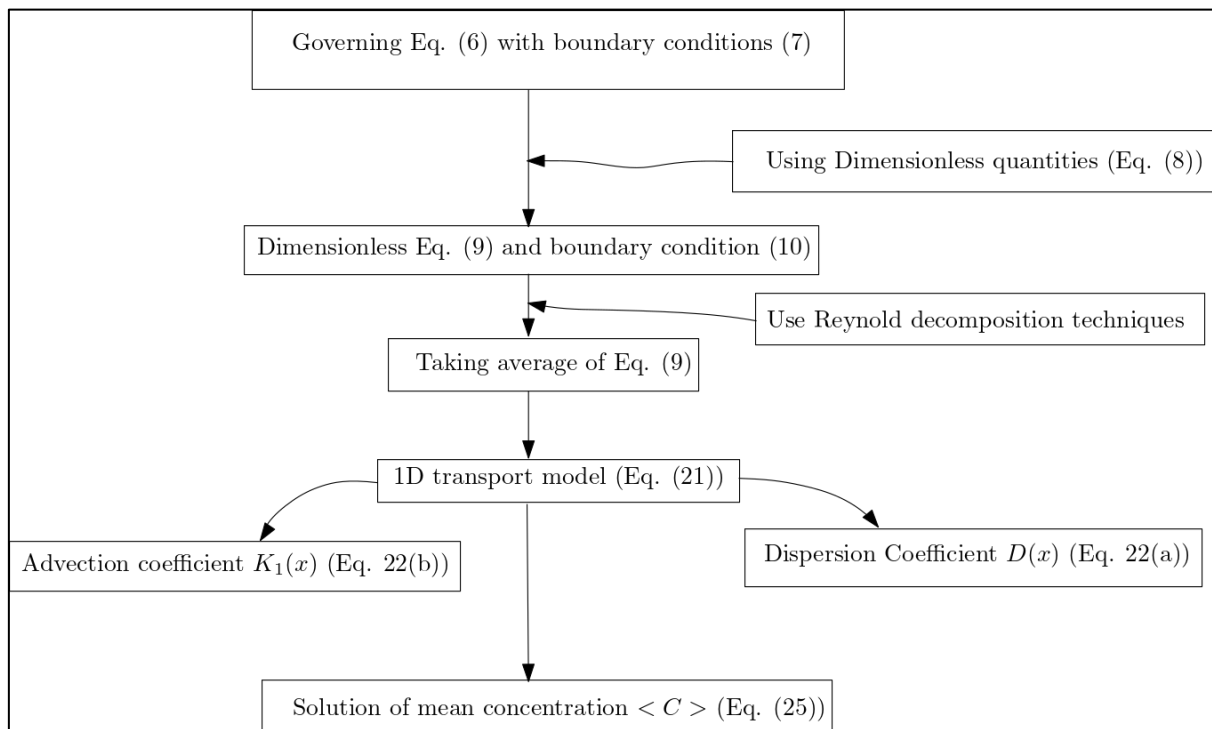


Fig. 2: Flowchart describing key stages of the analysis

## 3.Result and discussion

**Figures 3-9** illustrate the advection and dispersion characteristics computed for various peristaltic wave modulation and non-Newtonian power-law index parameters, along the channel length at fixed time.

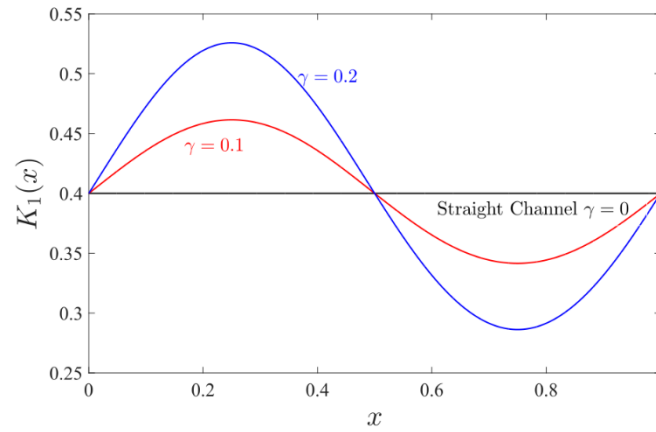


Figure 3: Advection coefficient against axial location, for various channel modulations,  $\gamma$ , for fixed  $Pe = 10, \delta = 0.5$

**Figure 3** shows that in the absence of peristalsis ( $\gamma = 0$ ) i.e., for the *straight rigid* channel, the advection coefficient is invariant along the channel length. With increasing modulation (peristaltic wave) parameter,  $\gamma$ , there is a strong elevation in advection coefficient in the initial half of the channel with a subsequent suppression in the second half of the channel, indicating that the *location* along the channel strongly influences advection (convective mass transfer) characteristics. This is associated with the expansion and contraction characteristics of the peristaltic motion. This is important since it shows that the average advection speed is constant irrespective of wave modulation for one period of wave oscillation.

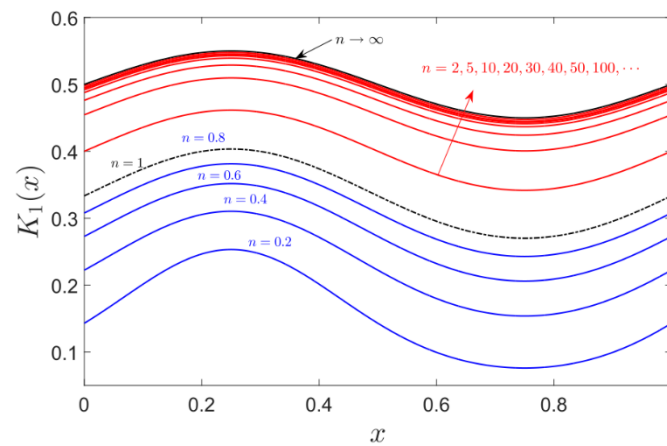


Figure 4: Advection coefficient against axial location, for various flow behavior index and fixed  $\partial p / \partial x = 1, \delta = 0.5, Pe = 10,$  and  $\gamma = 0.1$ .

**Figure 4** shows that advection coefficient is significantly elevated with increment in power-law rheological index (for shear-thinning fluids,  $n < 1$ ) across the channel length and exhibits an oscillatory nature due to the peristaltic waves which is consistent with Fig. 3. However much higher magnitudes are observed for dilatant i.e., shear-thickening blood ( $n > 1$ ). Slightly higher values are computed earlier along

the channel length with lower magnitudes observed further along the channel. At very high  $n$  values (dilatancy) the profiles do not subsequently alter tangibly.

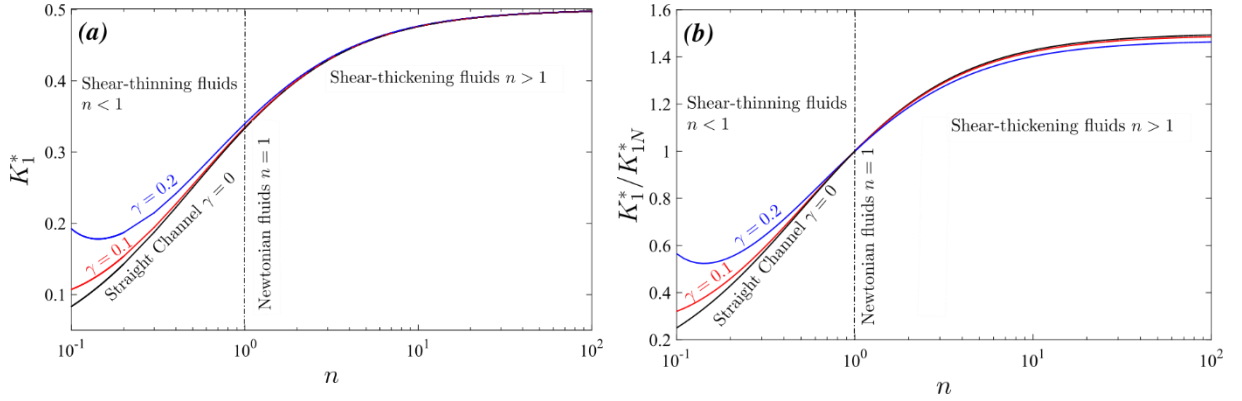


Figure 5: (a) Axially average advection coefficient and (b) axially average relative advection coefficient against flow behavior index for various channel modulations and fixed pressure gradient  $\partial p / \partial x = 1, \dot{\phi} = 0.5$  and  $Pe = 10$ .

**Figure 5** illustrates the collective influence of peristaltic modulation parameter and power-law index on (a) axially average advection coefficient and (b) axially average relative advection coefficient. In both plots the vertical dotted line indicates the Newtonian case ( $n = 1$ ) and no variation in either coefficient is computed for this case. In Fig 5a, for shear thinning fluids ( $n < 1$ ), initially with increment in modulation parameter,  $\gamma$ , there is a noticeable boost in axially averaged advection coefficient,  $K_1^*$  (the maximum elevation is computed for lowest power-law index of  $n = 0.1$ ); the trend is sustained for  $n < 1$ ; however, after the Newtonian case, as one enters the range  $n > 1$ , the effect is suppressed and eventually all profiles are observed to merge for  $n + 3$  (strongly dilatant behaviour). Minimal  $K_1^*$  values are computed at all values of  $n$  for the straight non-peristaltic case ( $\gamma = 0$ ). Clearly the advection process is enhanced for strongly pseudoplastic fluids whereas it is suppressed for strongly dilatant fluids. The rheology of blood therefore clearly modifies the advection behaviour. Figure 5b shows that similar trends are computed for the axially average relative advection coefficient  $K_1^*/K_{1N}^*$ , for pseudoplastic blood ( $n < 1$ ) i.e., the increase in peristaltic modulation parameter,  $\gamma$ , boosts the magnitude of the axially average relative advection coefficient. However, in the shear-thickening range ( $n > 1$ ), with progressive increase in  $n$ , an increment in peristaltic modulation parameter,  $\gamma$ , induces a marked reduction in the axially average relative advection coefficient  $K_1^*/K_{1N}^*$ . The greater viscosity of the dilatant blood contributes to this.

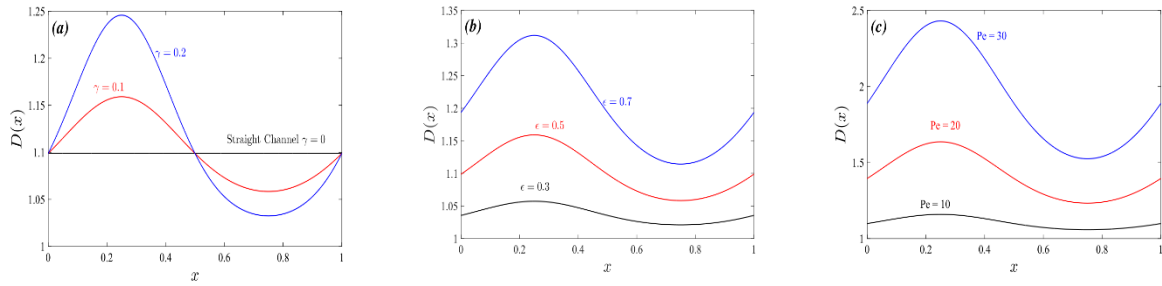


Figure 6: Dispersion coefficient against axial location, for (a) various channel modulations,  $\gamma$ , for fixed  $Pe = 10, \delta = 0.5$ , (b) various aspect ratio  $\delta$ , for fixed  $Pe = 10, \gamma = 0.1$ , and (c) various fixed Péclet number  $Pe$ , for fixed  $\gamma = 0.1, \delta = 0.5$ .

**Figure 6** illustrates the collective influence of (a) various channel modulations,  $\gamma$ , (b) various aspect ratio,  $\delta$ , and (c) various Péclet number  $Pe$ , on the dispersion coefficient,  $D(x)$ . In all the plots the sinusoidal nature of the peristaltic motion is clearly captured. Figure 6a shows that initially along the channel left half space, there is a boost in dispersion coefficient with increment in modulation parameter. The case of the rigid straight channel,  $\gamma = 0$  again exhibits no variation. However further long the channel, these trends are reversed, and the dispersion coefficient is decreased with greater modulation parameter. The peristaltic wave intensity therefore exerts a different influence on dispersion depending on whether contraction or expansion of the channel walls is occurring. Figure 6b shows that increasing aspect ratio  $\epsilon$ , i.e., length of channel relative to the depth, there is a significant elevation in the dispersion coefficient, in particular near the entry section to the channel. The enhancement in dispersion coefficient is however sustained throughout the length of the channel. Slender geometries of the blood vessel (i.e., length greater than depth, for example,  $\epsilon = 0.7$ ) contribute to assisting the hydrodynamic dispersion process whereas wider geometries (lower aspect ratio i.e.,  $\epsilon = 0.3$ ) induce the opposite effect. Figure 6c shows that with increasing Péclet number ( $Pe$ ), there is a substantial elevation in dispersion coefficient.  $Pe = \frac{v_{\text{wave}}\lambda}{D}$  and is directly proportional to the peristaltic wave speed on the channel walls. Essentially it expresses the relative contribution of convective (i.e., advective) and molecular diffusive transport phenomena in the blood flow. For  $Pe = 1$ , both mechanisms contribute equally. For  $Pe \gg 1$  advection dominates diffusion and this is the case examined in Fig. 6c. Increasing advection intensity clearly strongly assists the dispersion process at all locations, along the blood vessel (channel). All the plots correspond to the pseudoplastic case ( $n < 1$ ) and positive pressure gradient.

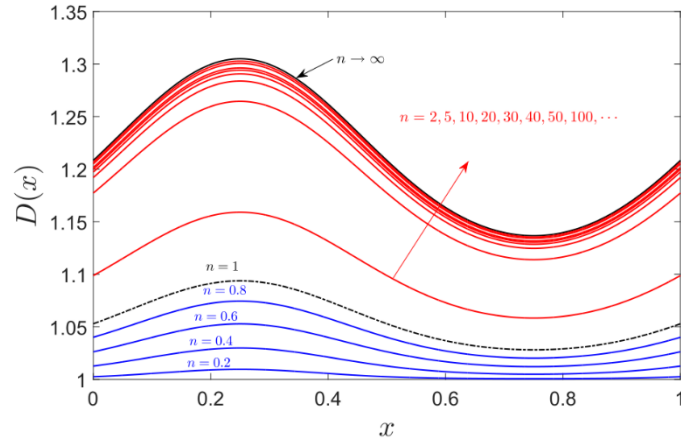


Figure 7: Dispersion coefficient against axial location, for various flow behavior index and fixed  $\partial p / \partial x = 1, \delta = 0.5, Pe = 10$ , and  $\gamma = 0.1$ .

**Figure 7** visualizes the impact of the rheological power-law index on the dispersion coefficient,  $D(x)$ . With stronger power-law fluids (lower  $n$  value), there is a suppression in the dispersion coefficient. With weaker power-law fluids (increasing  $n$ ) the dispersion coefficient is boosted. However, a much greater increment is computed in the dispersion coefficient with  $n > 1$  i.e., dilatant fluids. Shear thickening fluids therefore produce enhanced dispersion in the peristaltic blood flow compared with shear-thinning fluids. In all cases strong undulation is computed in the plots due to the peristaltic sinusoidal wave motion. Higher dispersion coefficient is generally observed earlier in the channel (blood vessel), closer to the entry zone, with much lower values computed further along the channel.

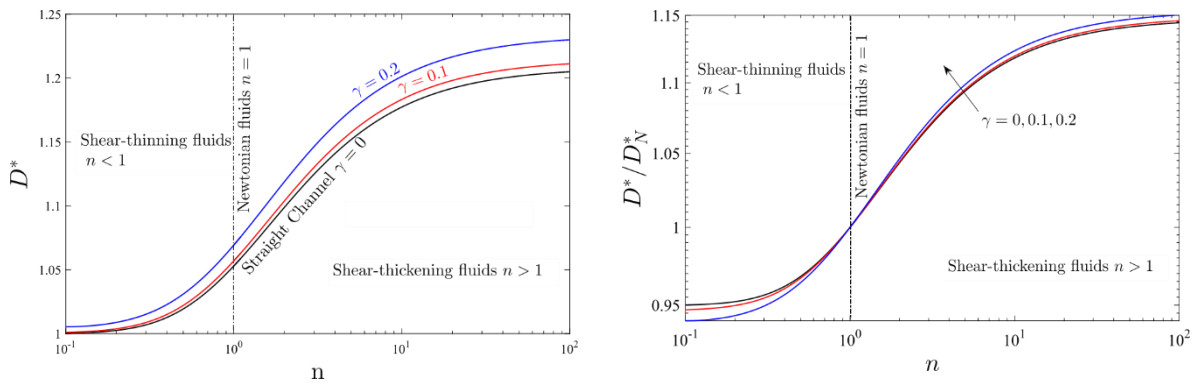


Figure 8: (a) Axially average dispersion coefficient and (b) axially average relative dispersion coefficient against flow behavior index for various channel modulations and fixed pressure gradient  $\partial p / \partial x = 1, \delta = 0.5$  and  $Pe = 10$ .

**Figure 8** displays the evolution in (a) axially averaged dispersion coefficient and (b) axially averaged relative dispersion coefficient against flow behavior index ( $n$ ) and various channel peristaltic modulation parameter ( $\gamma$ ). Figure 8a shows that at all values of power-law index ( $n$ ) there is a sharp increase in the axially averaged dispersion coefficient,  $D^*$ . This coefficient is minimized in the absence of peristalsis ( $\gamma = 0$ ). Overall, much greater magnitudes are computed for shear-thickening blood ( $n > 1$ ) compared with shear-thinning blood ( $n < 1$ ). For the case of Newtonian blood ( $n = 1$ ) a constant value of axially averaged dispersion coefficient is computed. The rheological characteristics of blood therefore strongly modify the

axial dispersion behaviour, which cannot be observed with the simple Newtonian model. Figure 8b reveals that for shear-thinning blood ( $n < 1$ ), a significant decrement in axially averaged relative dispersion coefficient  $D^* / D_N^*$  is present with increasing peristaltic modulation parameter ( $\gamma$ ). The opposite response is observed for shear thickening blood ( $n > 1$ ) where an enhancement in axially averaged relative dispersion coefficient  $D^* / D_N^*$  is computed. Clearly the much greater viscosity of dilatant (shear-thickening) blood contributes substantially to the boost in axial dispersion. Again, these plots correspond to the assistive pressure gradient case ( $\partial p / \partial x = 1$ ) with strong advection dominance ( $Pe = 10$ ) and intermediate aspect ratio of the channel ( $\epsilon = 0.5$ ).

Figure 9 depicts the distribution in mean concentration against axial distance at time  $t = 1$  for (a) for various channel modulations ( $\gamma$ ) and (b) for various flow behavior index values ( $n$ ). In Fig. 9a there is a marked elevation in mean concentration,  $\langle C \rangle$  as peristaltic modulation parameter is increased, indicating that more intense peristaltic wave motion at the channel walls enhances mean concentration. All profiles decay asymptotically from a maximum at the channel inlet ( $x = 0$ ) to vanish further along the channel length. Similarly in Fig. 9b there is a progressive increase in mean concentration  $\langle C \rangle$  with increment in power-law index. Mean concentration is depressed for strongly pseudoplastic blood ( $n = 0.2$ ) whereas it is boosted for strongly dilatant blood ( $n = 2, 5, 10$ ). The solute distribution in the blood vessel is clearly significantly modified depending on whether blood is shear thinning or shear thickening.

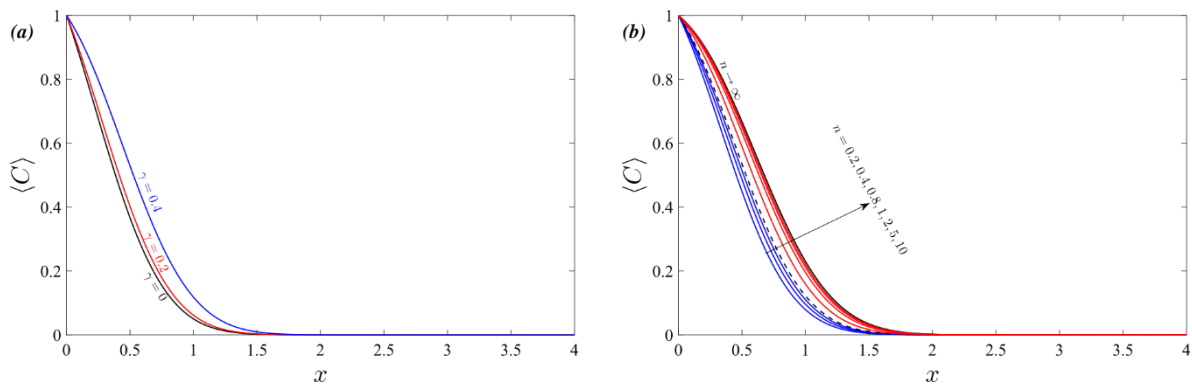


Figure 9: Mean concentration Vs axial distance at time  $t = 1$  for (a) variation of flow behavior index and fixed  $\partial p / \partial x = 1, \delta = 0.5, \gamma = 0.2$  and  $Pe = 10$  Axially average dispersion coefficient and (b) for various channel modulations and fixed pressure

## 4. Conclusions

A theoretical study has been conducted to analyse the unsteady solute convective-diffusive transport in non-Newtonian peristaltic blood flow in a two-dimensional channel (capillary). The power-law rheological model has been deployed and both pseudoplastic and dilatant blood has been considered. A velocity solution has been derived for generalized power-law index. *Reynolds' decomposition technique*

has been utilized in order to reduce the two-dimensional solute transport model into an equivalent one-dimensional model, in which the chemical species concentration and velocity in the channel have been considered as the sum of the cross-sectional average values and their deviations from the averages, enabling the extraction of the *dispersion coefficient and convection coefficient*. Using Fick's law, the advection-diffusion equation has then been modified by replacing these coefficients by their corresponding average values and analytical solutions for the mean concentration have been derived. The close formed solutions have been numerically evaluated in symbolic software. The principal findings of the present study may be summarized as follows:

- (i) In the absence of peristalsis effects ( $\gamma=0$ ) i.e., for the *straight rigid* channel, the dispersion coefficient is invariant along the channel length. With increasing modulation (peristaltic wave) parameter,  $\gamma$ , there is a strong elevation in advection coefficient in the initial half of the channel with a subsequent suppression in the second half of the channel, indicating that the location in the channel strongly influences advection characteristics.
- (ii) Advection coefficient is significantly elevated with increment in power-law rheological index (for shear-thinning fluids,  $n < 1$ ) across the channel length and exhibits an oscillatory nature due to the peristaltic waves.
- (iii) In the shear-thickening range ( $n > 1$ ), with progressive increase in  $n$ , an increment in peristaltic modulation parameter,  $\gamma$ , induces a marked reduction in the axially average relative advection coefficient.
- (iv) Dispersion coefficient is initially boosted along the early section of the channel with increment in modulation parameter whereas further long the channel this trend is reversed.
- (v) Increasing aspect ratio and Péclet number consistently boost dispersion coefficient along the entire channel length.
- (vi) Significantly higher magnitudes for axially averaged dispersion coefficient,  $D^*$  are computed for shear-thickening blood ( $n > 1$ ) compared with shear-thinning blood ( $n < 1$ ).
- (vii) A strong enhancement in mean solute concentration is induced with increasing peristaltic modulation parameter and for strongly dilatant blood. However, mean solute concentration is reduced considerably for strongly pseudoplastic blood.

The present study has considered a relatively simple non-Newtonian model for blood i.e., the power-law model, which has been shown to modify both advection and dispersion characteristics considerably in peristaltic flow. Future studies may explore alternative rheological models e. g. micropolar, Quemada, Carreau-Yasuda, bi-viscosity models etc, and may also include curved channel geometries. Also, it is very interesting to investigate nanoparticle transport [43, 44] as an extension of the present simulations for drug delivery applications. Efforts in these directions will be communicated imminently.

## Acknowledgements

Both the authors thank the anonymous referees for their useful suggestions.

## References

- [1] Krishnan, B.C., Rittgers, S.E. and Yoganathan A.P., *Biofluid Mechanics: The Human Circulation*, Taylor and Francis, New York, NY, USA (2012).
- [2] Jesudason, E.C., Smith, N.P., Connell, M.G., Spiller, D.G., White, M.R.H., Fernig, D.G. and Losty, P.D., Peristalsis of airway smooth muscle is developmentally regulated and uncoupled from hypoplastic lung growth, *American Journal of Physiology-Lung Cellular and Molecular Physiology*, 291(4), L559-565 (2006).
- [3] Miller, L.S., Kim, J.K., Dai, Q., Mekapati, J., Izanec, J., Chung, C., Liu, J.B., Sanderson, A., Bohning, M., Desipio, J. and Gandegok, J., Mechanics and hemodynamics of esophageal varices during peristaltic contraction, *American Journal of Physiology-Gastrointestinal and Liver Physiology*, 287(4), G830-G835 (2004).
- [4] Nisar, A., Afzulpurkar, N., Mahaisavariya, B. and Tuantranont, A. (2008). MEMS based micropumps in drug delivery and biomedical applications. *Sensors & Actuators, B*, 130(2), 917–942 (2008).
- [5] Jaggy, C., Lachat, M., Leskosek, B., Znd, G. and Turina, M., Affinity pump system: A new peristaltic blood pump for cardiopulmonary bypass. *Perfusion*, 15(1), 77–83 (2000).
- [6] Jaffrin, M. Y. Shapiro, A. H., Peristaltic pumping. *Annual Review of Fluid Mechanics*, 3, 13–37 (1971).
- [7] G. R. Cokelet, The rheology of human blood, in *Biomechanics*, Y. C. Fung et al., Ed., p. 63, Prentice-Hall, Englewood Cliffs, NJ, USA (1972).
- [8] Raju, K. K. and Devanathan, R., Peristaltic motion of a non-Newtonian fluid. *Rheologica Acta*, 11(2), 170–178 (1972).
- [9] Tripathi, D., Bég, O.A. and Curiel-Sosa, J.L., Homotopy semi-numerical simulation of peristaltic flow of generalized Oldroyd-B fluids with slip effects, *Computer Methods in Biomechanics Biomedical Engineering*, 17(4) 433-442 (2014).
- [10] Delouei, A.A., Nazari, M., Kayhani, M.H., Kang, S.K. and Succi, S., 2016. Non-Newtonian particulate flow simulation: A direct-forcing immersed boundary–lattice Boltzmann approach. *Physica A: Statistical Mechanics and its Applications*, 447, pp.1-20.
- [11] Jalali, A., Amiri Delouei, A., Khorashadizadeh, M., Golmohamadi, A.M. and Karimnejad, S., 2020. Mesoscopic simulation of forced convective heat transfer of Carreau-Yasuda fluid flow over an inclined square: Temperature-dependent viscosity. *Journal of Applied and Computational Mechanics*, 6(2), pp.307-319.

- [12] Afra, B., Delouei, A.A. and Tarokh, A., 2022. Flow-Induced Locomotion of a Flexible Filament in the Wake of a Cylinder in Non-Newtonian Flows. *International Journal of Mechanical Sciences*, p.107693.
- [13] Goud, J.S. and Reddy, R.H. A review chronicle of recent trends in peristaltic transport of non-Newtonian fluid. *International Journal of Pharmacy and Technology*, 8(4), 5118–5131 (2016).
- [14] Maiti, S. and Misra, J.C., Non-Newtonian characteristics of peristaltic flow of blood in microvessels. *Communications in Nonlinear Science and Numerical Simulation*, 18(8), 1970–1988 (2013).
- [15] Tripathi, D. and Bég, O.A., A numerical study of oscillating peristaltic flow of generalized Maxwell viscoelastic fluids through a porous medium, *Transport in Porous Media*, 95(2), 337–348 (2012).
- [16] Usha, S. and Ramachandra, R.A., Peristaltic transport of two layered power law of fluids. *ASME J. Biomechanical Engineering*, 119(4), 483–488 (1997).
- [17] Vajravelu, K., Sreenadh, S. and Babu, V.R., Peristaltic transport of a Herschel Bulkley fluid in an inclined tube. *International Journal of Non-Linear Mechanics*, 40(1), 83–90 (2005).
- [18] Ali, N., Javid, K., Sajid, M. and Bég, O.A., Numerical simulation of peristaltic flow of a biorheological fluid with shear-dependent viscosity in a curved channel, *Computer Methods in Biomechanics and Biomedical Engineering*, 19(6) 614–627 (2016).
- [19] Srivastava, L.M. and Srivastava, V.P., Peristaltic transport of blood: Casson model-II. *Journal of Biomechanics*, 17(11), 821–829 (1984).
- [20] Gudekote, M. and Choudhari, R., Slip effects on peristaltic transport of Casson fluid in an inclined elastic tube with porous walls. *Journal of Advanced Research in Fluid Mechanics and Thermal Sciences*, 43(1), 67–80 (2018).
- [21] Tripathi, D. and Bég, O.A., Mathematical modeling of peristaltic propulsion of viscoplastic fluids, *Proc. IMechE- Part H; J. Engineering in Medicine*, 228 (1), 67–88 (2014).
- [22] Taylor, G.I., Dispersion of soluble matter in solvent flowing slowly through a tube, *Proceedings of the Royal Society of London. Series A. Mathematical and Physical Sciences*, 219(1137), 186–203 (1953).
- [23] Aris, R., On the dispersion of a solute in a fluid flowing through a tube, *Proceedings of the Royal Society of London. Series A. Mathematical and Physical Sciences*, 235(1200), 67–77 (1956).
- [24] Gill, W.N. and Sankarasubramanian, R., Exact analysis of unsteady convective diffusion, *Proceedings of the Royal Society of London. Series A. Mathematical and Physical Sciences*, 316(1526), 341–350 (1970).
- [25] Lane, D.A. and Sirs, J.A., The dispersion of solutes during blood flow through a straight tube, *The Journal of Physiology*, 241(3): 689–698 (1974).
- [26] Caro, C.G., The dispersion of indicator flowing through simplified models of the circulation and its relevance to velocity profile in blood vessels, *The Journal of Physiology*, 185(3), 501–519 (1966).

- [27] Roy, A.K., Bég, O.A., Saha, A.K. and Murthy, J.V.R., Taylor dispersion in non-Darcy porous media with bulk chemical reaction: a model for drug transport in impeded blood vessels, *J. Engineering Mathematics*, 127(1), 1-18 (2021).
- [28] Fan, L.T. and Wang, C.B., Dispersion of matter in non-Newtonian laminar flow through a circular tube. *Proceedings of the Royal Society of London. Series A. Mathematical and Physical Sciences*, 292(1429), 203–208 (1966).
- [29] Dejam, M., 2018. Dispersion in non-Newtonian fluid flows in a conduit with porous walls. *Chemical Engineering Science*, 189, pp.296-310.
- [30] Shah, S.N., Cox, K.E., Dispersion of solutes in non-Newtonian laminar flow through a circular tube–Eyring model fluid. *Chemical Engineering Science*, 29(5), 1282–1286 (1974).
- [31] Sharp, M.K., Shear-augmented dispersion in non-Newtonian fluids. *Annals of Biomedical Engineering*, 21(4), 407–415 (1993).
- [32] Roy, A.K., and Bég, O.A., Mathematical modelling of unsteady solute dispersion in two-fluid (micropolar-Newtonian) blood flow with bulk reaction. *International Communications in Heat and Mass Transfer*, 122, 105169 (11 pages) (2021).
- [33] Bég, O.A. and Roy, A.K., Moment analysis of bi-component species transport with coupled reaction in non-Newtonian blood flow. *Chinese Journal of Physics*, 77, 1810-1826 (2022).
- [34] Saadun, N.H., Jaafar, N.A., Basir, M.F.M., Anqi, A. and Safaei, M.R., The effect of body acceleration on the dispersion of solute in a non-Newtonian blood flow through an artery. *International Journal of Numerical Methods for Heat & Fluid Flow*, 31(8), 2560-2579 (2021).
- [35] Rana, J. and Murthy, P.V.S.N., Unsteady solute dispersion in small blood vessels using a two-phase Casson model. *Proceedings of the Royal Society of London. Series A. Mathematical and Physical Sciences*, 473(2204), 20170427 (2021).
- [36] Ponalagusamy, R. and Murugan, D., Dispersion of a solute in blood flowing through narrow arteries with homogeneous first-order chemical reaction. *Proceedings of the National Academy of Sciences, India Section A: Physical Sciences*, 91(4), 675–680 (2021).
- [37] Radhakrishnamacharya, G. and Alemayehu, H., Dispersion of a solute in peristaltic motion of a couple stress fluid through a porous medium. *Tamkang Journal of Mathematics*, 43(4), 541 - 555 (2012).
- [38] Ravi Kiran, G., Radhakrishnamacharya, G. and Bég, O.A., Peristaltic flow and hydrodynamic dispersion of a reactive micropolar fluid: simulation of chemical effects in the digestive process. *Journal of Mechanics in Medicine and Biology*, 17(1), 1750013 (2017).
- [39] Scott Blair, G.W. and Spanner, D.C., *An Introduction to Biorheology*, Elsevier Scientific publication, Oxford, UK (1974).
- [40] Boyd, W., *Textbook of Pathology: Structure and Functions in Diseases*, Lea and Febiger, Philadelphia, Pa, USA (1963).

- [41] Bird, R.B., Stewart, W.E., Lightfoot, E.N. and Meredith, R.E., *Transport Phenomena*. John Wiley, New York (1960).
- [42] Ng, C.O. and Bai, Y.C., 2005. Dispersion in oscillatory Couette flow with sorptive boundaries. *Acta Mechanica*, 178(1), pp.65-84.
- [43] Bhatti, M.M., Sait, S.M., Ellahi, R., 2022. Magnetic nanoparticles for drug delivery through tapered stenosed artery with blood based non-Newtonian fluid. *Pharmaceuticals*, 15, p.1352.
- [44] Bhatti, M.M. and Abdelsalam, S.I., 2021. Bio-inspired peristaltic propulsion of hybrid nanofluid flow with Tantalum (Ta) and Gold (Au) nanoparticles under magnetic effects. *Waves in Random and Complex Media*, pp.1-26.